Research Article | Vol. 26, No. 22 | 29 Oct 2018 | OPTICS EXPRESS 28938
Optics EXPRESS

# Technique for generating periodic structured light beams using birefringent elements

ROLAND A. TERBORG,[1,*] JUAN P. TORRES,[1,2] AND VALERIO PRUNERI[1,3]

[1] *ICFO-Institut de Ciencies Fotoniques, The Barcelona Institute of Science and Technology, 08860 Castelldefels (Barcelona), Spain*
[2] *Department of Signal Theory and Communications, Universitat Politecnica de Catalunya, 08034 Barcelona, Spain*
[3] *ICREA-Institució Catalana de Recerca i Estudis Avançats, 08010, Barcelona, Spain*
[*] *roland.terborg@icfo.eu*

**Abstract:** We put forward a simple, scalable and robust technique for generating periodically structured light beams with intensity patterns, e.g. of the form $\cos^{2n}(k_x x)\cos^{2m}(k_y y)$, where $k_x$ and $k_y$ are real numbers that can be tailored and $n$ and $m$ are integers. The technique combines the use of Gaussian beams with curved wavefronts, birefringent crystals (Savart plates) and linear polarizers. Applications range from photolithography to fabrication of micro-lens array and fiber Bragg gratings, 3D printing and tailoring of optical lattices for trapping atoms and molecules.



## 1. Introduction

The use of periodic structured light patterns is a key element in many applications. They play an important role in several imaging technologies: 3D imaging of microscopic and macroscopic objects [1], biometric recognition in commercial mobile devices [2], and techniques for pushing the spatial resolution beyond the diffraction limit [3,4]. For fabrication of fiber Bragg gratings they are used to periodically modify the refractive index of the fiber, using the periodic patterns generated with two-beam interference [5]. Structured light beams appear also in atomic physics as optical lattices. This kind of beams acts as a versatile potential landscape to trap ultracold quantum gases of bosons and fermions that can be used, for instance, for quantum simulation [6].

For most of these applications, it is necessary to control and modify illumination properties such as the position of the whole beam, its periodicity and the orientation of the light pattern.

Spatial light modulators (SLMs) based on microelectromechanical systems and liquid crystal arrays are the most common instruments used for generating structured light. A more simple approach, based on two-beam interference, can be derived from Young's double pinhole experiment, which allows to generate intensity patterns of the form of $\sim cos^2(k_x x)$. Although versatile, SLMs are expensive, and in some cases their pixelated nature and limited phase control produce zero order diffraction beams and deteriorate the quality of the resulting beam. Additionally, most of these devices are not suitable for high power applications. Pinhole masks, on the other hand, may deliver a precise and smooth pattern, and they allow generating different kinds of illumination patterns [7]. However, they are not dynamic and show very low efficiency.

Here we introduce a technique that can generate several kinds of periodical patterns by using passive and inexpensive optical components such as linear polarizers and Savart plates. These components are ideal elements for producing interference even with low-coherence light [8], they are suitable for integration into a single compact device and for use with high-energy sources.

The technique presented here provides a wide variety of regular and scalable patterns, for example of the form of $cos^{2n}(k_x x + \alpha_x)cos^{2m}(k_y y + \alpha_y)$, where $\alpha_{x,y}$ are tunable phase shifts. We also show, as example of potential application, how these beams could be used for micro-structuring surfaces.

#338281 https://doi.org/10.1364/OE.26.028938
Journal © 2018 Received 10 Jul 2018; revised 27 Sep 2018; accepted 28 Sep 2018; published 24 Oct 2018

Optics EXPRESS

## 2. Description of the technique

A Savart plate (SP) is an optical element composed of two equal thickness plates of birefringent material cemented together, each with their optic axes at 45° to the surface normal and rotated 90° with respect to each other. Figure 1(a) depicts how the SP works. The SP splits an incoming beam with polarization along $(\hat{x}+\hat{y})/\sqrt{2}$ into two equal intensity beams, with orthogonal polarizations along $\hat{x}$ and $\hat{y}$, respectively. The two beams propagate parallel with a lateral displacement $S$. The displacement is determined by the illumination wavelength, the dispersion properties of the birefringent material and the thickness of the SP. When slightly tilted, the SP introduces an additional phase delay between the two orthogonal beams. This delay can range from zero to a few wavelengths without producing any other noticeable changes to the outgoing beams [8].

The SPs can be rotated. The orientation is determined by the line along which the two outgoing beams are displaced. In Fig. 1(a) the two beams that propagate parallel are displaced along $(\hat{y}-\hat{x})/\sqrt{2}$. We will show that by combining polarizers (Ps) and SPs with different orientations, we can generate controllable periodic intensity modulations. In Figs. 1(b) and 1(c) we show two examples of intensity patterns that can be generated with one or two SPs, and several Ps, chosen appropriately.

One essential ingredient of the technique is an input optical beam that, at the input face of the first SP, shows a curved wavefront. This is the case, for instance, of a Gaussian beam at a long distance from its beam waist, i.e., $z \gg z_R$, where $z$ is the longitudinal position along the beam, $z_R = kw_0^2/2$ is the Rayleigh range, $w_0$ is the beam waist and $k = 2\pi/\lambda$. In this case, the beam radius is $w(z) \sim w_0 z/z_R$ and the curvature is $R(z) \sim z$, so that the input electric fields $E_G$ reads

$$E_G = \frac{z_R E_0}{z} \exp\left[-\left(\frac{z_R}{w_0 z}\right)^2 r^2 + i\gamma r^2 - i\tan^{-1}\frac{z}{z_R}\right], \tag{1}$$

where

$$\gamma = \frac{\pi}{\lambda z}. \tag{2}$$

$r^2 = x^2 + y^2$ is the radial distance, $E_0$ is the amplitude of the electric field at the beam waist and $\tan^{-1} z/z_R$ is the Gouy phase shift. The polarization of the beam (not written explicitly for the sake of simplicity) is dictated by P1.

At the output face of the SP, two beams with orthogonal polarizations are generated, displaced by a distance $S$. The displacement can take place in an arbitrary direction given by vector $\mathbf{S} = S_x\hat{x} + S_y\hat{y}$, which is determined by the orientation of the SP. By appropriately tilting the SP, the beams can show a phase difference $\alpha$. Finally, a P projects the polarization of the two output beams into a common diagonal polarization.

Assuming that the separation between beams $S = \sqrt{S_x^2 + S_y^2}$ is much smaller than the beam size $(w_0 z/z_R)$ and that the axes of the Ps are aligned in a way such that the two beams are split and projected equally, the output beam after traversing SP1 and P2 [see Fig. 1(b)] reads

$$\begin{aligned} E_{out} = &\frac{1}{2}\frac{z_R E_0}{z} \exp\left[-\left(\frac{z_R}{w_0 z}\right)^2 r^2 - i\tan^{-1}\frac{z}{z_R}\right] \times \\ &\left\{\exp\left[i\gamma\left(x-\frac{S_x}{2}\right)^2 + i\gamma\left(y-\frac{S_y}{2}\right)^2 - i\frac{\alpha}{2}\right] + \right. \\ &\left.\exp\left[i\gamma\left(x+\frac{S_x}{2}\right)^2 + i\gamma\left(y+\frac{S_y}{2}\right)^2 + i\frac{\alpha}{2}\right]\right\}. \end{aligned} \tag{3}$$

Optics EXPRESS

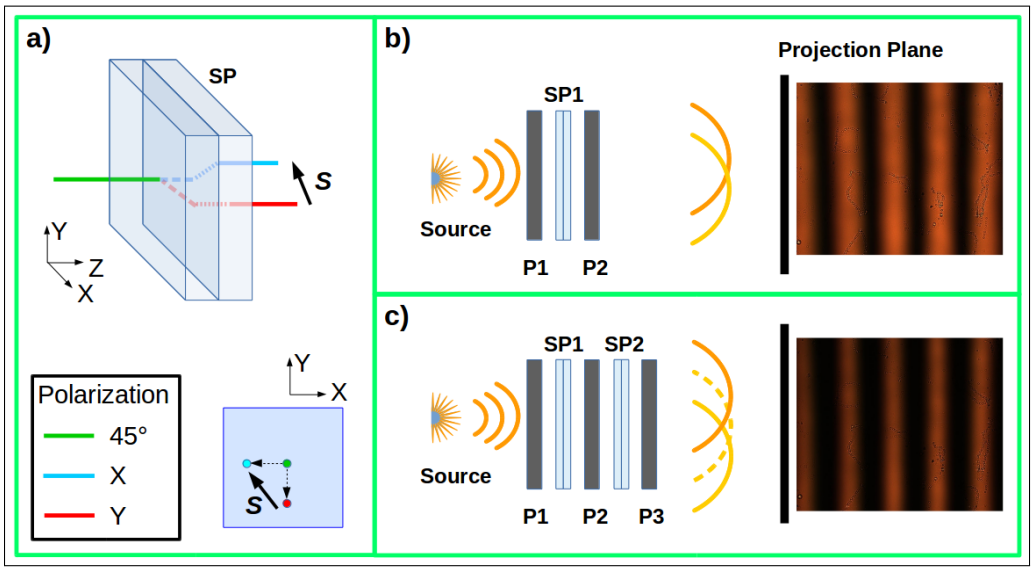


Fig. 1. Scheme of the proposed technique to generate structured light patterns: (a) A SP divides an input beam into two parallel outgoing beams with orthogonal polarizations, displaced each other laterally a distance $S$. (b) and (c) Experimental setups that include a light source, Savart plates SP1 and SP2 and linear polarizers P1,P2 and P3. The outgoing curved beams share the same polarization and interfere to generate intensity patterns of the form $cos^2(k_x x)$ and $cos^4(k_x x)$ in (b) and (c), respectively. $k_x$ and $k_y$ are real numbers that can be tailored by the technique.

which can be easily shown to be

$$E_{out} = E_G \exp\left[i\gamma\left(\frac{S_x^2}{4} + \frac{S_y^2}{4}\right)\right] \cos\left(\gamma\,\mathbf{S}\cdot\mathbf{r} + \frac{\alpha}{2}\right). \tag{4}$$

The intensity of the periodic pattern is written as

$$I_{out} = I_G \cos^2\left(\gamma\,\mathbf{S}\cdot\mathbf{r} + \frac{\alpha}{2}\right). \tag{5}$$

where $I_G = |E_G|^2$. The effect of the SP and the P on a linearly polarized input Gaussian beam with a large curvature is to produce a structured light beam with the original Gaussian intensity profile but modulated by a $\cos^2(\gamma\mathbf{S}\cdot\mathbf{r}+\alpha/2)$ pattern. Note that by controlling the phase difference $\alpha$ we can gradually change from a $\cos^2$ to a $\sin^2$ pattern. The same result can be achieved by rotating P1 or P2 by 90°, as this changes the sign of the polarization projection.

We can combine several SPs and Ps, with independent orientations, separation distances and phase shifts, to generate quite arbitrary patterns of light. Since there is no fundamental restriction to the number of SPs that we can concatenate, and to the orientation of each element, the technique provides numerous possibilities to generate multiple types of intensity profiles. This is an interesting property of the technique that allows to obtain intensity patterns of the form $cos^{2n}$, with $n$ being the number of SPs.

Let us consider some examples. We may have P1, followed by SP1 and P2, all oriented along $\hat{x}$. It produces a beam displacement $S_x$ between orthogonally polarized beams with a phase difference $\alpha_1$. A second SP (SP2) is oriented along $\hat{y}$ followed by P3 oriented along $x$, generating

Optics EXPRESS

two beams separated a distance $S_y$ with phase difference $\alpha_2$. After SP1 and P2, the field reads

$$E_{out_1} = E_G \exp\left(i\gamma \frac{S_x^2}{4}\right) \cos\left(\gamma\, S_x x + \frac{\alpha_1}{2}\right). \tag{6}$$

The second SP will only affect the $y$ coordinate so that, after P3:

$$E_{out_2} = E_G \exp\left[i\gamma\left(\frac{S_x^2}{4} + \frac{S_y^2}{4}\right)\right] \cos\left(\gamma\, S_x x + \frac{\alpha_1}{2}\right) \cos\left(\gamma\, S_y y + \frac{\alpha_2}{2}\right) \tag{7}$$

The resulting intensity pattern reads

$$I_{out_2} = I_G \cos^2\left(\gamma\, S_x x + \frac{\alpha_1}{2}\right) \cos^2\left(\gamma\, S_y y + \frac{\alpha_2}{2}\right). \tag{8}$$

A case of special interest is when the two SPs are oriented along the same direction, for instance $x$, generating each time two beams with separation $S_x$ but with independent phase differences $\alpha_1$ and $\alpha_2$. In this case the field after P3 reads

$$\begin{aligned} E_{out_3} = & \frac{E_G}{2} \exp\left[i\gamma\left(\frac{S_x^2}{2}\right)\right] \times \\ & \left\{\exp\left[-i\gamma S_x x - i\frac{\alpha_2}{2}\right] \cos\left(\gamma\, S_x(x - \frac{S_x}{2}) + \frac{\alpha_1}{2}\right) + \right. \\ & \left. \exp\left[i\gamma S_x x + i\frac{\alpha_2}{2}\right] \cos\left(\gamma\, S_x(x + \frac{S_x}{2}) + \frac{\alpha_1}{2}\right)\right\}. \end{aligned} \tag{9}$$

If the conditions

$$\alpha_2 = \alpha_1 + 2\mu\pi \tag{10}$$

and

$$\gamma = \frac{\nu\pi}{S_x^2} \tag{11}$$

are fulfilled, for $\mu$ and $\nu$ integer numbers, the intensity pattern of the output beam is written as

$$I_{out_3} = I_G^2 \cos^4\left(\frac{\nu\pi x}{S_x} + \frac{\alpha_1}{2} + \frac{\nu\pi}{2}\right). \tag{12}$$

We generate an intensity pattern of the form $\sim \cos^4$ for $\nu$ even, and a pattern of the form $\sim \sin^4$ for $\nu$ odd. According to the condition given in Eq. (11), these specific patterns can only exist at discrete propagation distances $z_\nu$:

$$z_\nu = \frac{S_x^2}{\nu\lambda} \tag{13}$$

The location of the pattern the farthest possible from the source is the one with $\nu = 1$, since the point corresponding to $\nu = 0$ lies at infinity. However, the term $\gamma S_x^2/\pi$ in Eq. (11) falls rapidly to zero over distance. With a propagation distance of only a few times $z_1$, we can already find a very good approximation to the $\cos^4$ pattern which will continue propagating to infinity.

The theoretical efficiency of the generation of these predefined beam geometries, in terms of output/input power, depends on the pattern, reaching a maximum of 50% for the one described in Eq. (5). However, a remarkable property of our technique is that the peak intensities of the patterns will maintain the original intensity values. In practice, the efficiency is also related to the number of optical elements traversed by the beam, especially Ps, since they produce power losses and, depending on their polarization contrast, can decrease visibility of the patterns. Commercially available elements like polarizing beam splitters with low absorption, anti-reflective coating and high polarization contrast considerably minimize the losses.

Optics EXPRESS

## 3. Generation of structurally stable intensity patterns

The periodic patterns of light generated in the first and second cases considered above are examples of structurally stable beams, since their transverse intensity distribution remains invariant, up to a scaling, under propagation [9, 10]. However, the pattern of light described in the third case considered only takes place at certain distances along the direction of propagation. Under which conditions do the optical beams generated correspond to structurally stable beams?

Figure 2 shows schematically the effect that a combination of SPs has on an incoming beam for three different cases. The three of them correspond to structurally stable beams. Dots represent the centers of the displaced outgoing beams that, before projection with a P, can have different polarization directions. Arrows indicate the beam displacement that generates the corresponding SP. Crosses represent those points where two or more outgoing beams overlap their centers.

We have found that only when i) all dots are contained in a circle, and ii) beams represented by crosses (beams with overlapping centers) outside of the circle show destructive interference, the resulting pattern will have structural stability. For the cases that do not fulfill this condition, the patterns will change periodically along the direction of propagation. For the case shown in Fig. 2(c) this implies that there should be a specific phase relationship between all phases ($\alpha_1$, $\alpha_2$ and $\alpha_3$) to guarantee that the two beams with overlapping centers represented by the cross at $\mathbf{x} = 0$ interfere destructively. A counterpart condition is not necessary for the cases shown in Figs. 2(a) and 2(b) where, regardless of phase relationships, since the beam centers are located inside a circle, there are no points depicted by crosses.

This result constitutes an interesting analogy with the condition that propagation invariant beams should fulfill. Only those patterns whose Fourier spectrum lies in the $(k_x, k_y)$ domain in a ring, i.e., $k_x^2 + k_y^2 = a^2$, will propagate without changing their structure [11–15]. The structurally stable patterns of the technique described here are visible at every propagation distance. The pattern is present only where the two beams overlap, leaving out the small regions where, due to the small displacement, the beams do not overlap. This is in contrast with the case of propagation invariant beams, like Bessel or Mathieu beams where, in real experiments, the desired pattern is only found within a confined region in the longitudinal direction.

It is possible to displace the generated beams in a continuous way by tilting the SPs or stepwise by rotating the Ps by $90^o$. The advantage of the latter method is that, contrary to the crystal tilting, it will be independent of the wavelength. By doing this we can easily switch from a pattern $I = E_G \cos^2(k_x x)\cos^2(k_y y)$ to $I = E_G \sin^2(k_x x)\cos^2(k_y y)$, $I = \cos^2(k_x x)\sin^2(k_y y)$ or $I = \sin^2(k_x x)\sin^2(k_y y)$, depending on which P is rotated.

A case of special interest is the one with three SPs, since, when properly aligned, they can produce the structurally stable hexagonal patterns shown in Fig. 2(c). We can spatially displace this pattern by applying a $\pi$-phase delay to the three SPs (or alternatively a $90^o$ rotation to the three Ps before them). We can also displace the pattern if we do this to only the first, only the second or only the third SP (or their corresponding P). These combinations will respectively give the intensity patterns $I_1$, $I_2$, $I_3$ and $I_4$ shown in Fig. 3. Since each of these patterns is structurally stable, a combination of exposures to these intensity patterns would result in a cumulative intensity pattern with a more complex structure, which would however preserve the same propagation invariance. Some examples of the possible combinations are the cumulative intensities $I_a$, $I_b$ and $I_c$ depicted in Fig. 3.

## 4. Experimental results

A setup similar to the ones shown in Figs. 1(b) and 1(c) were used to demonstrate experimentally the generation of some the intensity patterns described earlier. The light sources used were LEDs with central wavelengths $\lambda_R = 617nm$ (bandwidth of $18nm$ FWHM); $\lambda_G = 530nm$ ($33nm$) and $\lambda_B = 470nm$ ($25nm$). The input curved beam is a Gaussian beam that has been spatially filtered

Optics EXPRESS

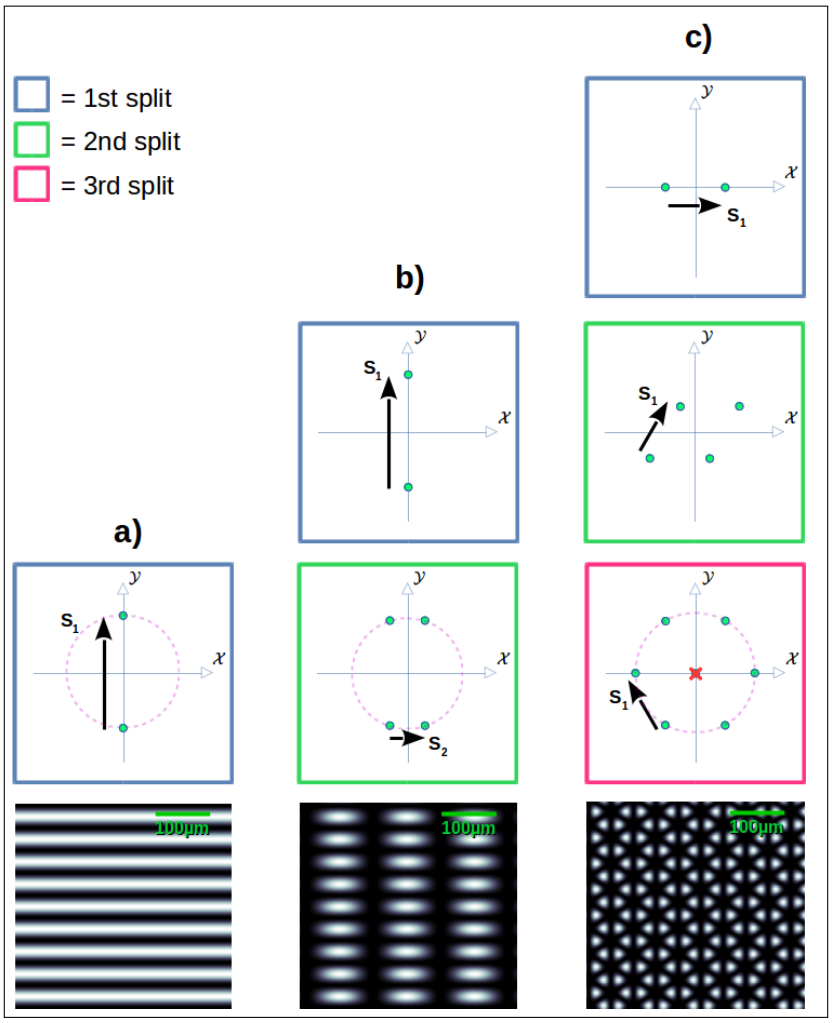


Fig. 2. Patterns of light generated and description of the splitting of the optical beams in each SP with: (a) one, (b) two and (c) three SPs. The green dots depict the position of the beam centers after each SP. The displacement generated by each SP is indicated by arrows. In (c) the red 'x' denotes where the centers of two beams overlap with an amplitude and phase relationship such that they interfere destructively. The dashed circles show that for these cases all the resulting points lie within a circle. In the text we show that these beams propagate preserving their structure. The bottom row shows the resulting output pattern for each case. Data: The input Gaussian beam (500 nm wavelength) shows a radius of curvature of $R = 5$ mm. The displacements introduced by the SPs are $S_1 = 60\mu m$ and $S_2 = S_1/3$).

by a pinhole of $300\mu m$ diameter. The light patterns were recorded with an image detector at the projection plane. In Fig. 4 we show different intensity patterns that can be obtained using two SPs.

In the profiles shown in Fig. 4(e) we can appreciate a modulation for the form $\sim \sin^4$ (green line) which becomes evident as it shows a narrower peak and broader valley than those of the form $\sim \sin^2$ (blue line). The beam curvature $R = 45mm$ for this pattern is 11 times larger than that for the modulations $\cos^4$ or $\sin^4$ with $\nu = 1$, meaning that in Fig. 4(c) we have only a good approximation of these states.

Optics EXPRESS

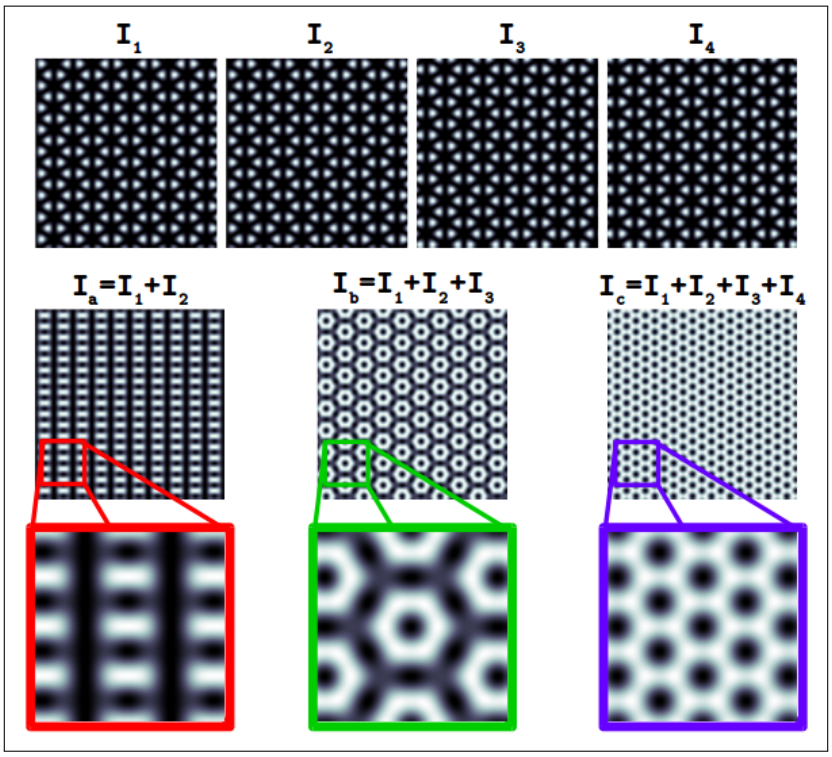


Fig. 3. Top row: Intensity patterns generated with three SPs after inducing a $\pi$-phase delay (or rotating the Ps by $90^o$) simultaneously to the three SPs ($I_1$), only to the first ($I_2$), only to the second ($I_3$) or only to the third SP ($I_4$). Center and bottom rows: Cumulative intensity patterns and close-ups from the resulting combinations: $I_a = I_1 + I_2$, $I_b = I_1 + I_2 + I_3$, $I_c = I_1 + I_2 + I_3 + I_4$.

Figures 4(f) and 4(g) demonstrate that this technique can easily be scalable, generating patterns that preserve their structure along the direction of propagation. Figures 4(h) and 4(i) show the potential of the proposed technique for generating a large variety of structures. These results show the capability of the presented technique to shape even low-coherence light sources. Due to the small separation of the beams and the nature of the elements used, the patterns are very stable against external perturbations, such as vibrations or air turbulences present in standard laboratory conditions.

## 5. Applications of the technique

Many current imaging technologies for tissue tomography and 3D scanning rely on the use of periodic light patterns with variable periodicity, position and wavelengths [1, 16, 17]. The technique that we put forward here clearly meets all these requirements, making it a potential candidate for use in imaging techniques.

For example, the technique allows engineering the shape of the spatially-dependent polarization of an optical beam. The role of Ps in the setup can be seen as filters that select the same polarization for the two displaced fields that initially bear orthogonal polarizations. If we discard, for example, P2 in the setup shown in Fig. 1(b), we will no longer detect changes in intensity across the beam. However the output polarization state will be linear and the corresponding vector will vary in space according to the form $[cos(\gamma Sx), sin(\gamma Sx)]$. The polarization states can therefore be modulated in a way similar to the intensity in order to obtain complex polarization distributions.

Optics EXPRESS

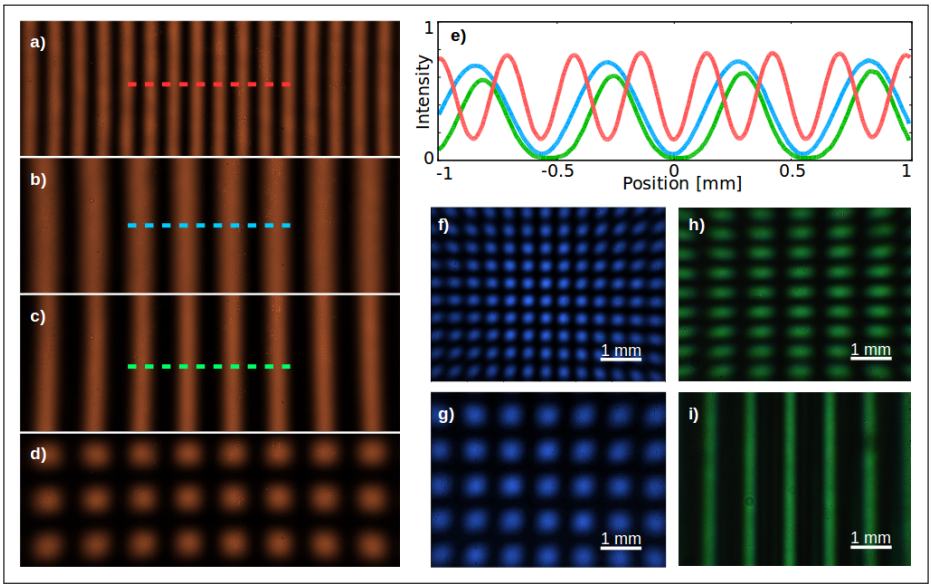


Fig. 4. Examples of structured illumination patterns. The illumination is at $\lambda_R = 617nm$, the beam curvature is $R = 45mm$, and and the displacements introduced by the SPs are $S = 50\mu m$ for SP1 and SP2. a) $I = \sin^2(2\gamma Sx)$ for a configuration [P1][SP1][SP2][P2], with SP1 and SP2 aligned to double the displacement to $2S = 100\mu m$; b) $I = \sin^2(\gamma Sx)$ with [P1][SP1][P2]: c) $I \approx \sin^4(\gamma Sx)$ with the configuration [P1][SP1][P2][SP2][P3]; d) $I = \sin^2(\gamma Sx)\cos^2(\gamma Sy)$. e) Intensity profile along the dotted lines in a), b) and c) (red, blue and green lines, respectively). f) and g) Experimental patterns of the kind $I = \cos^2(\gamma Sx)\cos^2(\gamma Sy)$ for an illumination at $\lambda_B = 470nm$ with beam displacements $S = 50\mu m$ and beam curvatures $R = 45mm$ and $R = 95mm$, respectively. h) and i) Patterns at $\lambda_G = 530nm$ of the kind $I = \cos^2(\gamma Sx)\cos^2(2\gamma Sy)$ and $I = (\cos(\gamma Sx) + \cos(2\gamma Sx))^2$ achieved with two different beam displacements $S_1 = 50\mu m$ and $S_2 = 100\mu m$ in orthogonal and in parallel directions.

Due to the versatility of the beams that can be generated, together with the robustness of the elements, we expect that the proposed technique could play an important role for surface micro-structuring, where large areas with periodic micro-patterns are needed, such as photolithography, micro-lens fabrication and 3D printing. Note also that the optical elements involved in this approach can have high damage thresholds, being a good alternative to spatial light modulators and other commercial devices.

In Fig. 5, we show a proof of concept experiment for photolithography and micro-lens production. UV light from an LED with a central wavelength $\lambda_{UV} = 385nm$ is used and a $\cos^2(k_x x)\cos^2(k_y y)$ modulation is applied to it (see Fig. 5(a). The light pattern is projected onto a glass slide covered with a uniform layer of a standard photo-sensitive polymer (AZ 5214 E, Microchemicals GmbH) used for photolithography. The polymer that is exposed to the UV light undergoes a chemical reaction that allows it to be removed with a solvent. After development, the polymer surface resembles the illumination profile. For the sake of clarity, in Fig. 5(b) we show a 3D scan of the negative of these cavities. The actual z-profile, measured along the blue line, is plotted in Fig. 5(d).

We could, for instance, use the resulting surface as a mold to cast a micro-lens array with a pitch of approximately $450\mu m$. By casting it on a material of refractive index $n = 1.5$, the expected focal length of each micro-lens would be around 4 cm. These parameters can be adjusted by placing the glass slide at a different distance, or by changing the pattern structure or

Optics EXPRESS

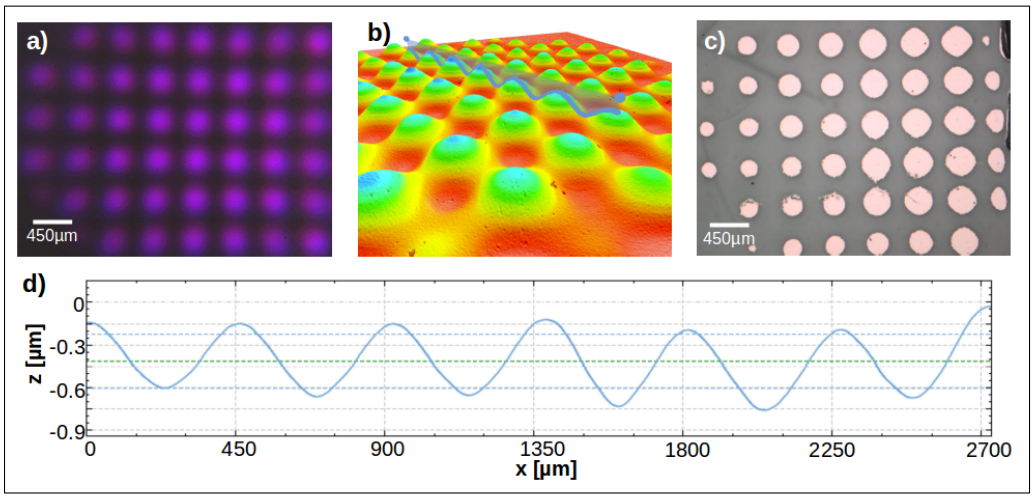


Fig. 5. Proof of concept surface structuring using the proposed technique: a) Illumination pattern of the form $I = \cos^2(\gamma Sx)\cos^2(\gamma Sy)$ used for writing (central wavelength $\lambda_{UV} = 385nm$ (FWHM=10nm). b) Negative 3D profile of the developed photo-sensitive polymer (AZ 5214 E, Microchemicals GmbH) after exposure to the illumination pattern (measured with SENSOFAR S neox Optical Profiler). c) Copper deposition on glass, revealing the over-exposed pattern on a photo-sensitive polymer. Variations in the intensity of the original beam lead to variations in the metallic spot sizes.

the exposure time. If we over-expose the polymer, the light pattern will produce regions where the glass is directly exposed. If we now deposit a material on the developed surface and dissolve the remaining polymer layer, the glass surface will be covered with the deposited material, revealing the shape of the intensity pattern. In Fig. 5(c), we see the results of applying this procedure and depositing copper on the over-exposed polymer. The copper circles are copies of the intensity pattern in Fig. 5(a). The different sizes in the pattern are due to differences in intensity in the illumination pattern. These show how, by changing the dose of light, one may also change the final structure.

In a similar way UV light patterns can be used for 3D printing techniques (for example with UV-curable resin), by growing periodic structures in layers. The system's ability to perform precise scanning means that more complex radiation patterns can be generated. In fact, the cumulative intensity pattern $I_c$ could be of particular interest for 3D printing since it allows to efficiently add a honeycomb micro-structure to be efficiently added to larger volumes, increasing stability and reducing the amount of needed material.

## 6. Conclusion

We have presented a novel technique for generating a variety of structured intensity patterns with low-coherence light. The technique has a simple implementation through birefringent elements (Savart plates), which split a curved beam and induce a lateral displacement. The Savart plates could be replaced by other birefringent elements, such as Nomarskii prism, Wollaston prism or stress-engineered optical (SEO) elements [18, 19].

We have theoretically studied the formation of periodic patterns, experimentally demonstrated several configurations, and, used one of them for surface micro-structuring. It presents several advantages with respect to alternatives for structured illumination, including spatial light modulators. For example, it can be applied to high energy optical sources requiring high damage threshold materials.

Optics EXPRESS

## Funding

Horizon 2020 Framework Programme (644956, 696656); North Atlantic Treaty Organization (NATO-SPS); Ministerio de Economía y Competitividad (SEV-2015-0522, TEC2016-75080-R); Generalitat de Catalunya (CERCA, ICREA); Agència de Gestió d'Ajuts Universitaris i de Recerca (AGAUR) (2017 SGR 1634); Fundación Cellex ; "la Caixa" Foundation (International PhD fellowship program "la Caixa"-Severo Ochoa @ ICFO)

## Acknowledgments

We would like to thank Prof. Miguel A. Alonso for valuable feedback and discussions. We also thank Dr. Josselin Pello and MSc. Melanie Cazaban for their help with some experiments.

## References

1. J. Geng, "Structured-light 3D surface imaging: a tutorial," Adv. Opt. Photon. **3**, 128–160 (2011).
2. Apple Inc., "Face ID," https://www.apple.com/iphone-x/#face-id (2018 (accessed May, 2018)).
3. M. G. L. Gustafsson, "Surpassing the lateral resolution limit by a factor of two using structured illumination microscopy," J. Microsc. **198**, 82–87 (2000).
4. L. Schermelleh, R. Heintzmann, and H. Leonhardt, "A guide to super-resolution fluorescence microscopy," J. Cell Biol. **190**, 165–175 (2010).
5. R. Kashyap, *Fiber bragg gratings* (Academic, 2009).
6. I. Bloch, "Ultracold quantum gases in optical lattices," Nat. Phys. **1**, 23–30 (2005).
7. R. Heintzmann, *Structured Illumination Methods* (Springer US, 2006), pp. 265–279.
8. R. A. Terborg, J. Pello, I. Mannelli, J. P. Torres, and V. Pruneri, "Ultrasensitive interferometric on-chip microscopy of transparent objects," Sci. Adv. **2**, e1600077 (2016).
9. E. Abramochkin and V. Volostnikov, "Spiral-type beams," Opt. Commun. **102**, 336–350 (1993).
10. E. G. Abramochkin and V. G. Volostnikov, "Spiral light beams," Phys.-Uspekhi **47**, 1177–1203 (2004).
11. J. Durnin, J. J. Miceli, and J. H. Eberly, "Diffraction-free beams," Phys. Rev. Lett. **58**, 1499–1501 (1987).
12. D. McGloin and K. Dholakia, "Bessel beams: Diffraction in a new light," Contemp. Phys. **46**, 15–28 (2005).
13. C. López-Mariscal, M. A. Bandres, and J. Gutiérrez-Vega, "Observation of the experimental propagation properties of helmholtz-gauss beams," Opt. Eng. **45**, 068001 (2006).
14. I. Ricardez-Vargas and K. Volke-Sepúlveda, "Experimental generation and dynamical reconfiguration of different circular optical lattices for applications in atom trapping," J. Opt. Soc. Am. B **27**, 948–955 (2010).
15. R. J. Hernández-Hernández, R. A. Terborg, I. Ricardez-Vargas, and K. Volke-Sepúlveda, "Experimental generation of mathieu–gauss beams with a phase-only spatial light modulator," Appl. Opt. **49**, 6903–6909 (2010).
16. D. J. Cuccia, F. Bevilacqua, A. J. Durkin, and B. J. Tromberg, "Modulated imaging: quantitative analysis and tomography of turbid media in the spatial-frequency domain," Opt. Lett. **30**, 1354–1356 (2005).
17. T. D. O'Sullivan, A. E. Cerussi, B. J. Tromberg, and D. J. Cuccia, "Diffuse optical imaging using spatially and temporally modulated light," J. Biomed. Opt. **17**, 071311 (2012).
18. R. D. Ramkhalawon, T. G. Brown, and M. A. Alonso, "Imaging the polarization of a light field," Opt. Express **21**, 4106–4115 (2013).
19. B. G. Zimmerman and T. G. Brown, "Star test image-sampling polarimeter," Opt. Express **24**, 23154–23161 (2016).